PFG 2013 / 6, 0603–0617
Stuttgart, December 2013

Report

Advanced High Resolution SAR Interferometry of Urban Areas with Airborne Millimetrewave Radar

Michael Schmitt, München, Christophe Magnard, Zürich, Schweiz, Stephan Stanko, Wachtberg, Christian Ackermann & Uwe Stilla, München

Keywords: synthetic aperture radar (SAR), SAR Interferometry, multi-aspect, airborne, urban areas, millimetrewaves

Summary: For rural and natural scenes, synthetic aperture radar interferometry (InSAR) has long been an operational technique for the generation of digital surface models. With the advent of sensors providing data in the decimetre resolution domain, also the analysis of densely built-up urban areas has become an increasingly important research topic. Due to the complexity of this kind of scenes, however, advanced interferometric techniques have to be employed. While usually satellite-borne stacks of multi-temporal data are collected in order to make use of differential SAR interferometry or the increasingly popular persistent scatterer technique, this article aims at the utilization of an airborne single-pass multi-baseline system working in the millimetrewave domain. Starting from the description of the exemplary German MEMPHIS sensor, the complete processing chain from the collection of necessary navigation data over the focusing of the raw SAR data to finally the application of sophisticated InSAR techniques is shown.

Zusammenfassung: *Fortgeschrittene hochauflösende SAR Interferometrie urbaner Szenen mit flugzeuggetragenem Millimeterwellen Radar.* Für ländliche und natürliche Szenen ist die SAR-Interferometrie seit langem eine operationelle Technik zur Generierung digitaler Oberflächenmodelle. Mit dem Einzug von Sensoren, die Daten im Dezimeter-Bereich bereitstellen, ist auch die Analyse dicht bebauter städtischer Gebiete ein zunehmend wichtiges Forschungsthema geworden. Wegen der Komplexität dieser Art von Szenen müssen jedoch fortgeschrittene interferometrische Techniken verwendet werden. Während dazu üblicherweise von Satelliten aus aufgenommene Stapel multi-temporaler Daten gesammelt werden, um sich der differentiellen SAR-Interferometrie oder der zunehmend populären Persistent Scatterer-Technik zu bedienen, zielt dieser Artikel auf die Verwendung eines flugzeuggetragenen Einpass-Mehrfachbasislinien-Systems ab, das im Millimeterwellenbereich arbeitet. Ausgehend von der beispielhaften Beschreibung des deutschen MEMPHIS-Sensors wird die komplette Prozessierungskette von der Aufnahme der benötigten Navigationsdaten über die Fokussierung der rohen SAR-Daten hin zur Anwendung hochentwickelter InSAR-Techniken gezeigt.

1 Introduction

The derivation of the topography of extended areas by across-track synthetic aperture radar (SAR) interferometry has been operational for quite some years now (Bamler & Hartl 1998, Rosen et al. 2000). New spaceborne missions with resolutions in the metre-range like the German TanDEM-X or the Italian COSMO-Skymed satellites have led to a growing number of applications also for urban areas that have not been in the scope of lower resolution data before (Stilla 2007, Sörgel 2010). While spaceborne SAR systems are typically operated in L-, C- or X-band, it is reasonable to employ shorter wavelengths in the millimetrewave domain (Ka-band or W-band) in order to maximize the achievable height estimation ac-

www.schweizerbart.de
DOI: 10.1127/1432-8364/2013/0199
1432-8364/13/0199 $ 4.00

curacy even for limited baselines enabling the design of single-pass multi-baseline systems mounted on airborne platforms.

Together with the general ability of airborne sensors to realize almost arbitrary flight track configurations (in contrast to the fixed ascending/descending orbital geometry of most satellite sensors), this allows the utilization of advanced SAR interferometry methods like multi-baseline phase unwrapping, SAR tomography or multi-aspect data fusion, which greatly supports the reconstruction of digital surface models (DSMs) of complicated urban areas without the need to collect multi-temporal data stacks over relatively long periods of time. This is particularly interesting for time-critical disaster mapping scenarios.

Apart from these methodical capabilities, millimetrewave SAR provides additional convenient characteristics in comparison to X-band SAR, e.g. inherently low speckle and a larger amount of non-specular backscattering due to the higher sensitivity for surface roughness. Besides these, with millimetrewave SAR it is possible to generate high-resolution images with short synthetic aperture, while the systems can be miniaturized and therefore be adapted to unmanned aerial vehicles (UAVs), see for example (Edrich & Weiss 2008, Nouvel & Plessis 2008, Stanko et al. 2012).

This article presents the experimental German MEMPHIS system as an example for airborne millimetrewave SARs, although it has to be mentioned that first plans for spaceborne missions exist (Schaefer et al. 2012). Exploiting the high flexibility of airborne systems, the main focus of this paper is put on a high resolution interferometric analysis of urban scenes with the final goal of DSM reconstruction in mind. Starting from a description of the system's hardware, the sensor characteristics and the setup in the aircraft, the complete processing chain from the focusing of the raw data with the aid of a high-precision inertial navigation system (INS) to the exploitation of multi-baseline and multi-aspect data is shown. In this context preliminary results are presented based on real test data acquired during a flight campaign over the city of Munich, Germany, in 2011.

2 Interferometric SAR Analysis of Urban Areas – State of the Art

Since SAR interferometry was introduced in the the 1970s (Graham 1974), it has continuously attracted the attention of an interdisciplinary research community. From plain single- or repeat-pass interferometry of natural and rural scenes via differential interferometric analysis of geophysical phenomena like earthquakes or volcanoes (Gens & Van Genderen 1996) to the sophisticated persistent scatterer technique (Ferretti et al. 2001) it has evolved to an operational remote sensing technology that has become indispensable to the earth observation and geoinformation communities. Among the most important developments is the ongoing improvement of imaging resolutions. While state-of-the-art spaceborne missions are now able to deliver data in the metre or even sub-metre domain, modern airborne sensors provide imagery with resolutions of down to several centimetres (Brenner 2010). With the advent of this kind of very high and ultra high resolution sensors a detailed interferometric analysis of urban areas has become possible. However, due to the SAR inherent side-looking geometry, the exploitation of (interferometric) SAR data for the reconstruction of urban digital surface models needs sophisticated processing strategies and is still a commonly investigated topic in the research community (Stilla et al. 2003, Bamler et al. 2009, Schmitt et al. 2011, Rossi et al. 2012). While much of the early work was based on model-driven image analysis in order to cope with or even exploit imaging effects like layover or shadowing (Bolter 2001, Thiele et al. 2007), the derivation of point clouds by persistent scatterer interferometry (PSI) has drawn growing interest during the last decade (Gernhardt et al. 2010). The main advantage of this framework is that only quasi-deterministic scatterers, whose reflectivities remain stable during a set of multi-temporal acquisitions, are considered for the analysis, thus leading to an enhanced point quality. Furthermore, in this way also information about the movement of these persistent scatterers can be derived – and remote sensing of four dimensions becomes possible. Since many repeat-pass images are needed for PSI, usually spaceborne

data is utilized for this technique. By fusing PSI point clouds from image stacks acquired by both ascending and descending satellite tracks as proposed by Gernhardt et al. (2012), densely sampled 3D and even 4D point data of whole cities can be derived.

Another promising development in the field of SAR interferometry over urban areas is the utilization of array signal processing techniques for multi-baseline data, which can either be employed in order to realize real 3D imaging by the formation of so-called SAR tomograms or to separate multiple discrete scattering contributions whose signals were mixed in one resolution cell due to the layover effect. Recently, many propitious approaches have been proposed in this field, e.g. based on airborne PolInSAR data for detailed urban scatterer characterisation (Sauer et al. 2011). The latest improvement was the introduction of compressive sensing based algorithms, which provide an efficient means for the separation of discrete scattering contributions in layover resolution cells and were even adapted to the four-dimensional imaging of extended city areas (Zhu & Bamler 2010, Reale et al. 2011).

Although obviously much progress has been made and a detailed imaging of urban areas by means of synthetic aperture radar has become a valuable remote sensing tool, some drawbacks remain: First of all, the core advantage of SAR remote sensing is the independence on daylight and weather conditions, making it especially interesting for time-critical tasks such as disaster mapping. However, this unique capability is lost if repeat-pass data have to be collected over relatively long periods of time. Furthermore, repeat-pass data suffer from temporal decorrelation, which eventually leads to a loss in coherence of the InSAR data and thus makes the related phase measurements less reliable. The second drawback is the SAR inherent side-looking imaging geometry that not only leads to the already-mentioned layover effect but also to radar shadowing causing areas without exploitable information in the images. An intuitive solution for this problem is the utilization of data from different aspect angles. However, state-of-the-art satellite missions only allow for the fusion of ascending and descending data stacks, i.e. two aspects, which only partly helps to achieve comprehensive information. Therefore, this paper wants to emphasize the strengths of airborne single-pass multi-baseline InSAR systems: Using such systems, highly coherent data from almost arbitrary aspect angles can be acquired in very short time, thus providing the full advantages and flexibilities of radar remote sensing.

3 Millimetrewave SAR System Characteristics

The potential of advanced InSAR processing strategies exploiting millimetrewave system peculiarities is investigated based on experimental data acquired on a flight campaign in May 2011. During this campaign, an interferometric four-antenna configuration with a maximum baseline span of 27.5 cm was employed. The utilized airborne sensor, MEMPHIS, is described in section 3.1, and details about the interferometric configuration can be found in section 5.1. As illustrated in Fig. 1, the test scene, located in the Maxvorstadt neighbourhood of the city of Munich, Germany, was illuminated from a full multi-aspect configuration consisting of five orthogonal and anti-par-

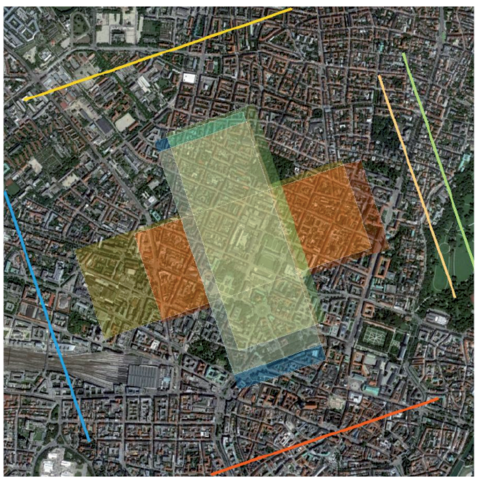

Fig. 1: Trajectories of the flight campaign Munich 2011. Note that the two tracks on the right to the scene were carried out at two different flying heights. Thus, a full multi-aspect configuration with an additional fifth acquisition was realized (Optical image ©2012 Google).

allel flight tracks. The goal of this campaign was to create an exemplary dataset of airborne multi-aspect multi-baseline InSAR data using a millimetrewave sensor in order to promote the development of advanced processing strategies necessary for urban area analysis.

3.1 *The MEMPHIS Sensor*

MEMPHIS (Millimeterwave Experimental Multifrequency Polarimetric High-resolution Interferometric System) was developed by the Fraunhofer Institute for High Frequency Physics and Radar Technology FHR in 1998 (Schimpf et al. 2002). The radar system uses two front-ends of identical architecture, and operates at 35 GHz and 94 GHz (Ka-band and W-band), respectively. The primary frequencies of 25 GHz and 85 GHz are generated by successive multiplication and filtering of the reference frequency of 100 MHz. For both subsystems the waveform is modulated onto an auxiliary signal at 9.4 GHz, which is upconverted into the respective frequency band together with the primary signal. Depending on the application, the sensor can either be used with polarimetric monopulse feeds or an interferometric set of four receiving antennae. The elevation-azimuth asymmetry of the beam that is necessary for SAR applications is achieved by aspheric lenses in front of the feed horns. Being an experimental, modular and removable system, MEMPHIS is typically mounted on a C-160 Transall airplane of the German Armed Forces (see Fig. 2). Due to various possible antenna shapes and configurations, data can be acquired in many different SAR modes: single-pass multi-baseline cross-track interferometry with four receiving antennas, dual-pol circular or linear polarimetry and even monopulse for moving target indication (MTI).

Fig. 2: MEMPHIS radar mounted into a C-160. Top: Synergy infrared optical sensor, center: 35 GHz interferometric SAR antenna with 3° × 13° beamwidth (box), bottom: 94 GHz polarimetric monopulse antenna with 1° × 13° beamwidth.

3.2 *Millimetrewave Peculiarities*

Due to the fact that typical wavelengths of millimetrewave frequencies differ from more common radar remote sensing bands (L, C, X) in about one order of magnitude, several peculiarities have to be considered; some of them can be exploited advantageously. The main advantages of millimetrewave systems certainly are two-fold: First of all, they allow for a significant miniaturization of the hardware, thus enabling the use on unmanned aerial vehicles (UAVs) and other small-scale carrier platforms. Second, very high resolutions may be achieved with comparably short synthetic apertures. One of the advantages resulting from a short synthetic aperture is that images of vegetation will be better focused, because blurring caused by movements of leaves and branches etc. is reduced.

Additional peculiarities of millimetrewaves in comparison to conventional microwave regions occur in the fields of atmospheric propagation and surface roughness and are explained in the following. A more detailed summary of millimetrewave specifics can be found in Essen (2010).

3.2.1 Propagation through the atmosphere

For millimetrewave radar applications, mainly the transmission windows around 35 GHz and 94 GHz are employed, whereas high propagation losses prohibit long range applications (> 10 km). The millimetrewave region is nevertheless an interesting alternative to the more common X-band due to considerably different

propagation properties (Skolnik 1980), which are caused by resonance absorption at these frequencies related to energy levels of vibration and rotation states of molecules in the atmosphere, e. g. water vapour or oxygen.

In remote sensing, the propagation through snow, fog, haze or clouds is one of the most important reasons why SAR sensors are used. While in optical remote sensing the drop size within fog and clouds is in an order of magnitude where interactions with the electromagnetic radiation of the visible spectrum is most likely, these effects are of much minor importance for millimetrewaves. As long as the density of droplets is not too high, and as long as the liquid water content of snow is not excessively high, millimetrewave signals are able to penetrate most weather phenomena. Only hydrometeors with high density of large drop sizes in the order of the electromagnetic wavelength can severely influence the propagation of the signal and thus prevent the desired imaging of the Earth surface (Danklmayer & Chandra 2009). This is caused by the fact that the drops act as antennae in this case, absorbing the energy of the resonant electromagnetic wave.

For the case of smoke first experiments show a low attenuation for millimetrewaves, due to the small particle size of smoke in comparison to e. g. sand or dust. In these latter cases, experimental results can be used for an estimation of the expected propagation loss. These attributes make millimetrwaves almost just as interesting for any kind of mapping or reconnaissance mission during disaster scenarios, be it floodings (mostly in concurrence with clouds and rainfall), dust storms or fires.

It has to be mentioned however, that even within the millimetrewave domain differences between the different frequencies appear. For example, in W-band the attenuation significantly increases with high temperatures and humidity; it therefore is often used in weather radars (Liebe 1985). For that reason, the choice of the band eventually depends on the mission goal.

3.2.2 Surface roughness properties

In the millimetrewave region, the wavelength is naturally very short in comparison to classical radar bands, i. e. the relating phase reacts very sensitively on movements of objects or the radar itself. While this might seem disadvantageous for a signal processing based imaging system that relies on the evaluation of the phase of the backscattered signal, it can be utilized beneficially instead. The reason is the specific scattering mechanism, which is dominated by a comparably much rougher surface (factor of 10 in comparison to X-band), making millimetrewave SAR more robust against uncontrolled movements of the carrier aircraft. In general, the roughness of surfaces causes diffuse scattering, whereas smooth surfaces result in specular reflections. At millimetrewave frequencies, most surfaces appear rough, and diffuse scattering dominates the images (see Tab. 1). Diffuse scattering leads to coherent averaging, an effect similar to multilook processing. Therefore, the inherent speckle effect within scenes of homogeneous surface structure is lower at millimetrewave frequencies than at X-band for an equal amount of multilook processing. Besides this primary advantage of higher roughness sensitivity, another one is the larger extent of rough appearing surfaces in often rather smooth urban environments. This provides a convenient benefit to the analysis of backscattering characteristics, which is often based on the assumption of Gaussian scattering. Since this assumption only holds for so-called distribut-

Tab. 1: Definition of radar roughness categories. The RMS surface height variations (cm) at a local incidence angle of 45° are shown (after Lillesand et al. 2004)

	Ka-band (λ = 0.86 cm)	X-band (λ = 3.2 cm)	L-band (λ = 23.5 cm)
Smooth	< 0.05	< 0.18	< 1.33
Intermediate	0.05 – 0.28	0.18 – 1.03	1.33 – 7.55
Rough	> 0.28	> 1.03	> 7.55

ed scatterers and not for frequently occurring point scatterers, millimetrewaves are favourable over longer wavelengths, where tendentially surfaces appear less rough and therefore more point scattering behaviours or specular reflections are observed.

3.3 *Navigation Systems*

Since the precision of the aircraft navigation data is not sufficient for high-precision SAR processing, for the 2011 campaign the system was complemented with a dGPS system composed of a GPS L1/L2 antenna (AeroAntenna AT2775-41) coupled to a receiver running at 20 Hz sampling rate (Trimble R7) and a precise INS working at 500 Hz sampling rate (iNAV-RQH from the company IMAR). The GPS, INS and SAR systems were synchronised through event markers and secondary markers with the GPS time. The realization of time synchronisation for the IMU was carried out by the pulse per second (PPS) signal and NMEA information of the GPS receiver. The navigation solution of the GPS and IMU data was then processed with the commercial software Inertial Explorer using dGPS data from reference base stations (Waypoint Products Group 2013). The navigation data were finally smoothed with a Kalman filter to avoid small variations in the millimetre range, which would introduce artefacts in the focused SAR data. The lever arms between the dGPS antenna, the INS and the SAR antennas fixed in operating position were measured using terrestrial surveying methods with a few centimetres accuracy.

4 SAR Raw Data Processing

MEMPHIS is a stepped-frequency radar system, where the pulse length can be adjusted in the range of 80 ns – 2 µs. For the high-resolution mode, it successively transmits 8 chirps of 200 MHz bandwidth with a 100 MHz carrier frequency shift between each other, thus building together a 900 MHz full bandwidth, resulting in a range resolution of about 16.5 cm. As described in Magnard et al. (2012), the raw data from each chirp are first focused in range using a chirp replica with the conventional matched filtering technique. The full bandwidth is reconstructed in the frequency domain through an algorithm based on Lord (2000) and Wilkinson et al. (1998). The azimuth compression is performed with the Extended Omega-K algorithm (Reigber et al. 2006), resulting in a zero-Doppler slant range geometry. The block diagram in Fig. 3 shows the processing chain of the algorithm.

One of the most critical steps for reaching high focusing quality and geolocation accuracy is the motion compensation, which can be divided in a first and a second order step; the geometry is shown in Fig. 4.

The first order motion compensation is achieved as follows:

- The navigation data are upsampled to the pulse repetition frequency (PRF) rate.
- A linearized track is defined using a least squares method on the position data in

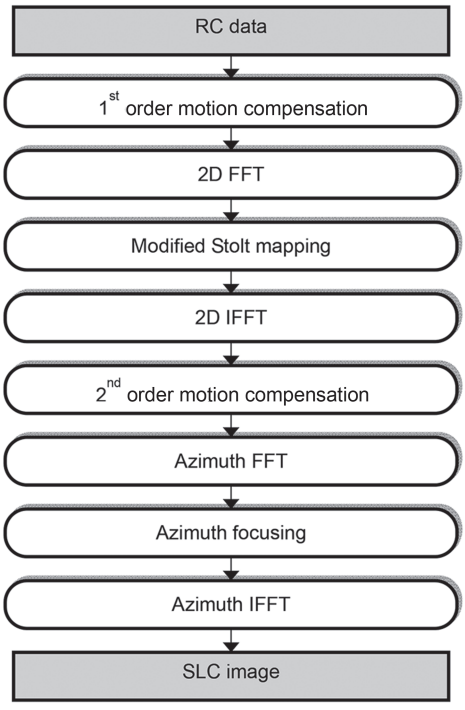

Fig. 3: Block diagram of the Extended Omega-K algorithm (FFT = fast Fourier transform, IFFT = inverse fast Fourier transform, SLC = single look complex).

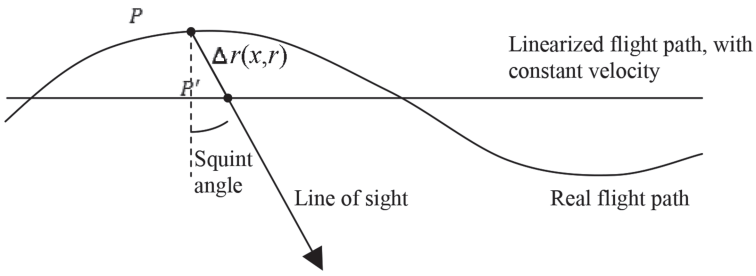

Fig. 4: Geometry of the motion compensation. The plane represented in the sketch is a plane formed by the linearized flight path and the line of sight.

global Cartesian coordinates. A constant linearised velocity is defined.

- For each echo, the projection of the vector $\overrightarrow{PP'}$ linking the real and the linearized track onto the mid-range line of sight is evaluated. The result corresponds to the first order range correction $\Delta r(x,r_m)$ in Reigber et al. (2006), with x the azimuth position and r_m the mid-range distance. The phase and position in the range direction of the range-compressed (RC) data are corrected according to this value.
- The RC data are interpolated in azimuth direction according to the constant linearized velocity, getting a regular (constant) spatial azimuth sampling.

The second order motion compensation consists of the following procedure:

- The vector linking the real and linearized track is projected onto the line of sight of each range sample (using a flat reference surface), yielding the second order range correction $\Delta r(x,r)$ used in Reigber et al. (2006), with r being the range distance. The difference between this projection and the one applied in the first order motion compensation is used for correcting the phase and position of the data.

The motion compensation works best for objects at the reference surface. The more the objects are above or below this surface or the larger the difference between the real and the linearized flight path is, the larger the geolocation errors and the focusing degradation will be.

5 Advanced SAR Interferometry Applications

In this section, the application of MEMPHIS data as an example for a single-pass multi-baseline millimetrewave InSAR system is shown with respect to advanced InSAR analysis and a focus on the reconstruction of digital surface models of urban areas. Since modern sensors are able to provide SAR imagery in the decimetre-resolution class, the interferometric analysis of densely built-up inner city areas has challenged the remote sensing community. This is especially caused by the SAR inherent side-looking imaging geometry that produces effects like layover and shadowing, making the interpretation of (In)SAR imagery of urban scenes a non-trivial task. While shadowing leads to image patches without exploitable information, layover on the one hand leads to difficulties in the phase-unwrapping stage of classic SAR interferometry, and on the other hand causes signal mixtures of different backscatterers, e.g. roof and wall of a building together with the ground in front of the building. A sketch illustrating these effects can be found in Fig. 5.

5.1 *Multi-baseline InSAR*

5.1.1 Phase unwrapping

The multi-baseline configuration of MEMPHIS can conveniently be exploited for the phase unwrapping stage during a standard InSAR processing chain. In order to do so, the fact that the four receiving antennae can be

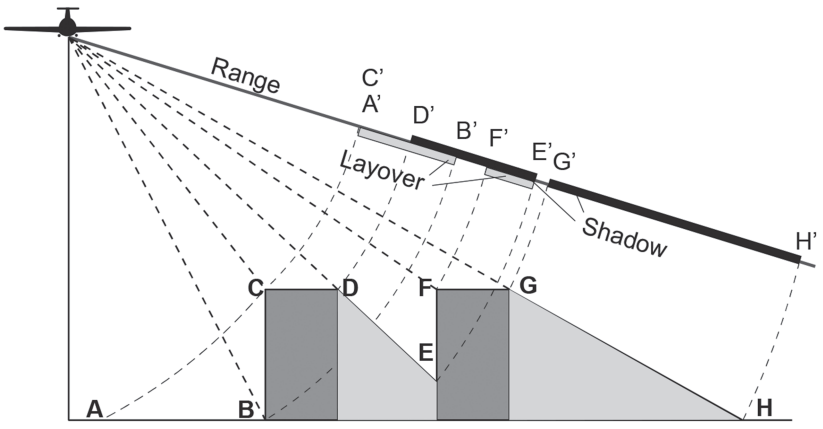

Fig. 5: Sketch of the imaging effects caused by the SAR inherent side-looking imaging geometry. Note, for example, how the roof CD of the left building partially mixes with the backscattering of the façade BC and the ground AB.

used to form five different baselines is exploited. The height ambiguities

$$h_a = \frac{\lambda R \sin\theta}{B\cos(\theta-\alpha)} \tag{1}$$

for the different baselines can be found in Tab. 2. R is the slant range, θ the off-nadir angle, B the baseline, and α the baseline inclination.

For multi-baseline phase unwrapping, a coarse-to-fine approach was proposed by Essen et al. (2007). As a reference, the phase given by the interferogram with the largest ambiguity height, i. e. the shortest baseline is used, as it often does not require being unwrapped itself. The interferograms generated using longer baselines are then successively unwrapped with the help of the phase information from the already unwrapped interferograms.

The phase unwrapping of the fine interferogram is a two-step process: First, the phase of the reference interferogram $\phi_{i,ref}$ is calibrated to match the phase of the fine interferogram $\phi_{i,fine}$ by computing a phase offset ϕ_{offset} that minimizes the following expression:

$$\min_{\phi_{offset}\in[-\pi;\pi]}\left[\sum_i\left(\left(\phi_{i,ref}\cdot\frac{B_{fine}}{B_{ref}}+\phi_{offset}\right)\bmod 2\pi-\phi_{i,fine}\right)^2\right] \tag{2}$$

with B_{ref} and B_{fine} being the baseline lengths of the reference and fine interferograms, respectively. This offset is necessary since all interferograms as shown in Tab. 2 are created, which are not all based on the same master antenna. Once ϕ_{offset} has been determined, the fine interferogram is unwrapped:

$$\phi_{i,fine,unwrapped} = \left\lfloor \frac{\phi_{i,ref}\cdot\frac{B_{fine}}{B_{ref}}+\phi_{offset}-\phi_{i,fine}}{2\pi}+0.5 \right\rfloor \cdot 2\pi+\phi_{i,fine} \tag{3}$$

Possible errors are corrected with the addition or subtraction of 2π, while taking care that the gradients between neighbouring pixels stay in the interval [−π–ε; π+ε], where ε is the phase noise. This process is conducted on the first pair of interferograms with baselines B_1 for the reference interferogram and B_2 for the fine interferogram. It is then repeated using the resulting unwrapped phase map as the reference interferogram and the next interferogram with baseline B_3 as the fine interferogram, and so on, until the interferogram

with the longest baseline is unwrapped. An example of the unwrapping is shown in Fig. 6.

Tab. 2: Typical ambiguity heights for the Ka-band antenna of MEMPHIS at mid-range (1631 m), sensor altitude: 715 m above ground level, baseline inclination: 65°.

Receiving antennas	Baseline (cm)	Height ambiguity (m)
R_1, R_2	B_1 = 5.5	227.7
R_2,R_3 or R_3,R_4	B_2 = 11.0	113.9
R_1,R_3	B_3 = 16.5	75.9
R_2,R_4	B_4 = 22.0	56.9
R_1,R_4	B_5 = 27.5	45.6

5.1.2 Layover separation and tomography

Layover separation can either be seen as a multi-baseline extension of classic single-baseline interferometry or as a special case of SAR tomography (TomoSAR). TomoSAR is based on the establishment of a synthetic aperture in elevation direction by exploitation of stacked coregistered images acquired from slightly different viewing angles. In contrast to the synthetic aperture that is employed for azimuth focusing, the tomographic (elevation) aperture can only make use of a sparse and irregularly sampled aperture – which is especially tough for the single-pass MEMPHIS case with just four samples (coming from the four receiving antennas) per resolution cell. It is well known, e.g. Reigber & Moreira

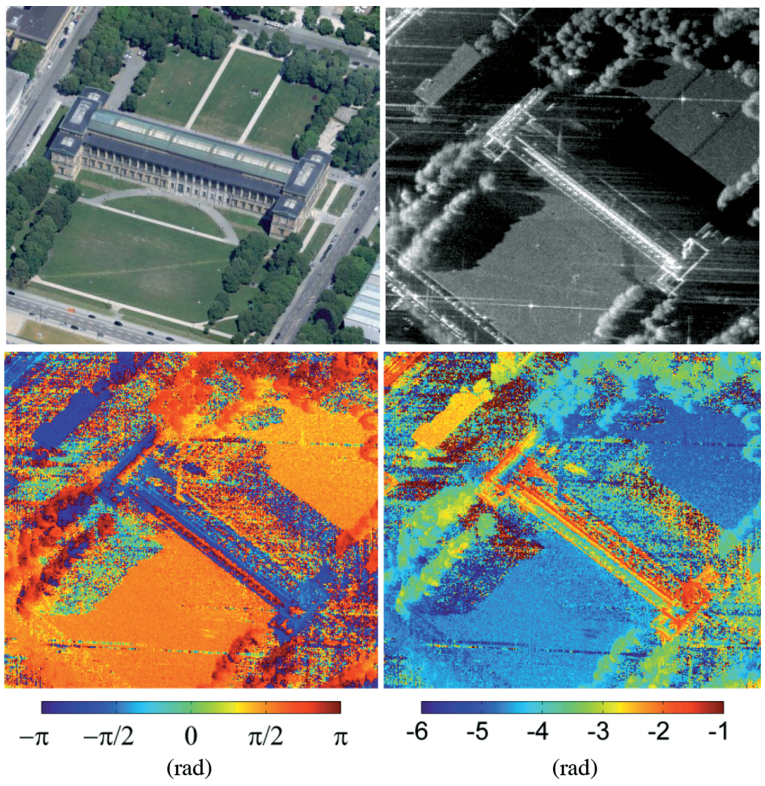

Fig. 6: The top-left image is an oblique-view aerial image and shows the “Alte Pinakothek” in Munich, Germany. The top-right image shows a SAR amplitude image of the same building acquired in 2011. The bottom-left image shows the corresponding interferogram with the largest baseline (27.5 cm), and the bottom-right image shows the same interferogram after the phase unwrapping process (Optical image ©2012 Google).

(2000), that the expected height resolution of single-pass multi-baseline InSAR systems is given by

$$\rho_h = \frac{\lambda R \sin(\theta)}{\Delta B}. \quad (4)$$

Since ΔB equals to the overall baseline length, and $\theta \approx \alpha$ for MEMPHIS, the height resolution equals to the height ambiguity as calculated using (3) and shown in Tab. 2 for the longest baseline B_5, namely ca. 45 m. Since this resolution is far worse than the achievable azimuth and range resolutions, the reflectivity profiles of the resolution cells are usually estimated using spectral analysis methods with super-resolution capabilities, e. g. MUSIC (multiple signal classification) (Schmidt 1986). A first example based on application of MUSIC-based spectral estimation to an urban scene can be seen in Fig. 7. The processing is organized as follows:

- First, the complex covariance matrix is estimated for every pixel of the stack using an adaptive filter proposed in Schmitt & Stilla (2013b).
- Next, the covariance matrix is eigen-decomposed in order to separate the eigenvectors belonging to noise space E_N from the eigenvectors belonging to signal space E_S.
- Using the steering vector

$$\vec{a}(h) = \exp\left(-j\frac{2\pi}{\lambda}\cdot\frac{B_{\perp,n}}{R\sin(\theta)}h\right) \quad (5)$$

where λ denotes the wavelength, $B_{\perp,n}$ is the perpendicular baseline between the master antenna and antenna n, R is the slant range distance, θ is the off-nadir angle, and h is

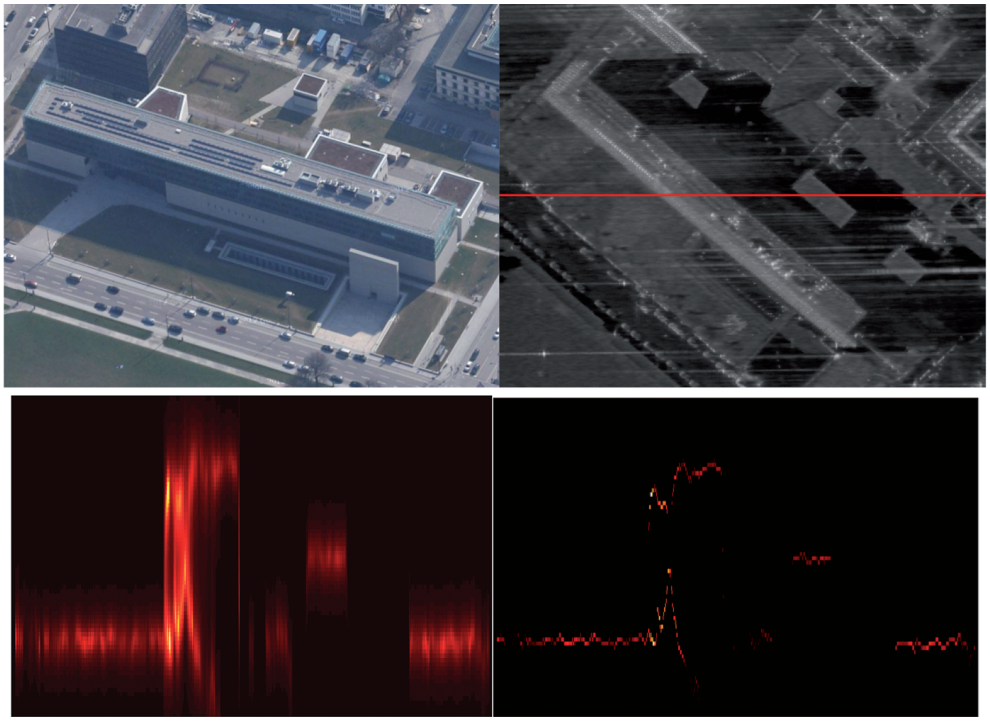

Fig. 7: Single-pass TomoSAR results for a test building in the city of Munich, Germany. The top-left image shows an oblique view aerial image of the building, the top-right image displays the SAR intensity image and the azimuth profile under investigation (red line). The bottom images show tomographic slices: The continuous MUSIC pseudo-spectrum is displayed on the left, the discrete scattering profile is displayed on the right. Note the double scatterers that have been detected in the layover part (Optical image ©2012 Google).

the height above the reference surface, the MUSIC pseudo-spectrum

$$P_{MUSIC}(h) = \frac{1}{\vec{a}^H(h) E_N^H E_N \vec{a}(h)} \quad (6)$$

is estimated for every resolution cell. The superscript H denotes the conjugate transpose.

For the visualization in Fig. 7, the continuous MUSIC pseudo-reflectivities are displayed for one azimuth slice. Although these results are just preliminary, they show a promising perspective for future investigations in more advanced SAR tomography methods.

Basically, both TomoSAR and layover separation rely on the same principles. The main difference is that TomoSAR intends to reconstruct the full, possibly continuous reflectivity profile for each resolution cell in order to realize real 3D imaging for example for scenes with volume scattering, whereas layover separation is the utilization of multi-baseline SAR interferometry for the separation of discrete scatterers whose backscattering has mixed due to the layover effect. It is well-known that single-pass systems are theoretically able to retrieve the heights of K = N – 1 scatterers (N: number of receiving antennae), which means that MEMPHIS should be able to separate the information of up to three height contributions within one resolution cell. Using simulated test data, Schmitt & Stilla (2013a) have shown that methods like distributed compressive sensing should be able to successfully reconstruct discrete backscattering profiles containing two point scatterers from a height separation of about 12 m – 13 m for sufficiently high signal-to-noise ratio (SNR).

Fig. 8: Zoom into the area of interest used for the illustrations in Figs. 9 and 10 (Optical image ©2012 Google).

If discrete scatterers are to be detected using the MUSIC procedure described above, their height can be determined by

$$\hat{h} = \max_h P_{MUSIC} \quad (7)$$

The resulting profile of discrete scattering points is also shown in Fig. 7. Obviously, some double scatterers caused by layover have been detected and resolved successfully, although the resolution capability seems to become worse with shrinking height difference between the scatterers.

5.2 *Multi-Aspect Data Fusion*

As has been mentioned before, the shadowing effect leads to gaps in the reconstructed height data if only one single dataset is used. A promising approach to cope with this problem is the utilization of images recorded from different aspect angles (see Fig. 1). In this way, on the one hand potential gaps can be filled with complementary data, while on the other hand redundant measurements can be exploited to enhance the final reconstruction accuracy. The advantage of single-pass interferometric data is that shadowing can easily be detected by looking for pixels showing low coherence. In order to show the significance of multi-aspect InSAR configurations, the backward geocoding procedure as proposed in Schmitt & Stilla (2011) is employed: First, the desired mapping grid is defined in the world coordinate system of choice, e.g. UTM. Then, each grid element is extended to the height dimension with a pre-defined height spacing in order to receive a set of height hypotheses. Each height hypothesis is then projected into one or more available aspects using the inverted, linearized range-Doppler equations:

$$t = \frac{(\mathbf{p} - \mathbf{s}_o)\mathbf{v}}{\|\mathbf{v}\|^2} \quad (8)$$

$$R = \|\mathbf{p} - \mathbf{s}\| \tag{9}$$

Where $\mathbf{p} = [x \;\; y \;\; z]^T$ denotes the 3D hypothesis, $\mathbf{s}_0 = [x_{s0} \;\; y_{s0} \;\; z_{s0}]^T$ describes the master antenna position during acquisition of the first azimuth bin, and $\mathbf{v} = [v_x \;\; v_y \;\; v_z]^T$ is the three-dimensional velocity vector of the master antenna. Then, the interferometric phase $\phi_{measured}$ is measured for the projected pixel and compared to the expected (simulated) interferometric phase

$$\phi_{simulated} = \left\langle -\frac{2\pi}{\lambda}\left(\|\mathbf{p} - \mathbf{s}_M\| - \|\mathbf{p} - \mathbf{s}_{Sl}\|\right)\right\rangle_{2\pi}, \tag{10}$$

where $\mathbf{s}_M$ and $\mathbf{s}_{Sl}$ denote the positions of the master and the slave sensor, respectively, and $\langle\,\rangle_{2\pi}$ denotes the wrapping operator. Finally, the height hypothesis that leads to the smallest difference between measured and simulated phase is kept as the actual height value of the grid element. If more than one dataset, i. e. aspect, is available, the height value can be chosen according to the mean difference between simulated and measured phase values weighted by the corresponding coherence values, such that redundant observations are exploited for each grid element. The weighting by coherence enables that only reliable phase measurements are considered, while shadow pixels (with typically low coherence) do not influence the result significantly.

Fig. 9 shows the scene converted into a binary map with all potential shadow pixels being displayed in black. It can clearly be seen how the combination of multiple aspects enhances the overall coverage of the area. While 58.6% of the scene are occluded due to shadowing in the single aspect case, using a joint analysis of multiple aspects leads to a low amount of non-information pixels of just 14.4%. These remaining non-information pixels are partly caused by narrow street canyons and possibly also by specular reflections.

The raw 2.5D DSM resulting from the fusion of five aspects acquired from crossing and anti-parallel trajectories at two different heights (see Fig. 1) is shown in Fig. 10.

In addition to conventional multi-aspect configurations, Palm et al. (2012) have recently shown how circular trajectories can be used as the supreme form of multi-aspect SAR imaging: The circular trajectory is just cut into overlapping sub-tracks of 2.5°, i. e. in total more than 140 MASAR (multiple aspect SAR) images are generated. It is, however, still an open question how many views are needed in order to realize the ideal multi-aspect configuration.

6 Conclusion and Outlook

In this article, the utilization of an airborne single-pass multi-baseline SAR system for advanced interferometric SAR analysis of complex urban scenes has been described; furthermore, the benefit of radar technology in the

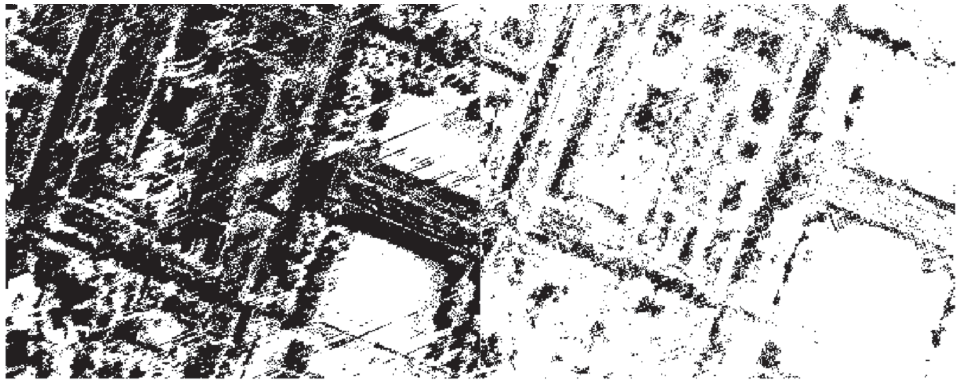

Fig. 9: Pixels for which no or only unreliable phase measurements are available are shown in black, high coherence pixels are shown in white. Left: one aspect alone. Right: five aspects merged. Note the improvement of the amount of available information by multi-aspect data fusion.

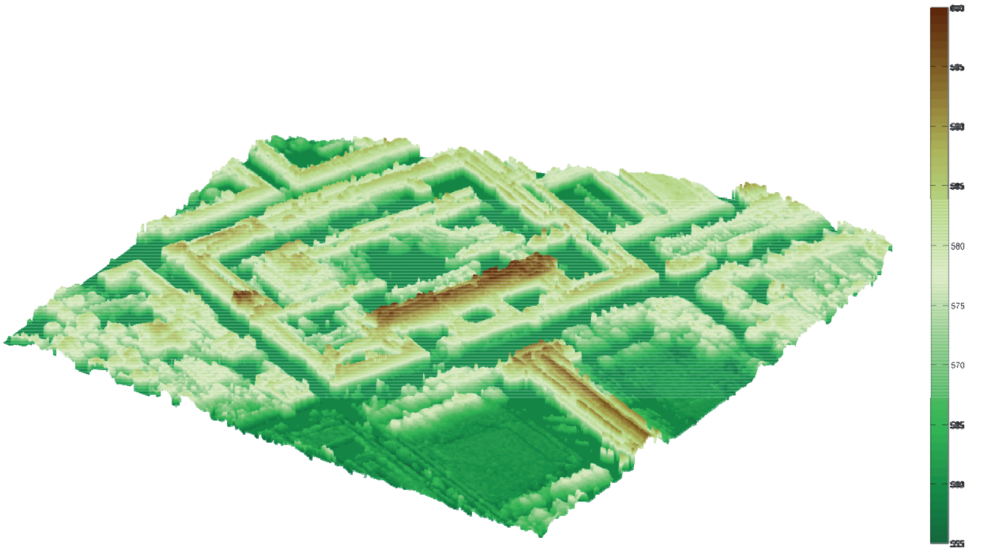

Fig. 10: Digital surface model as a result of multi-aspect InSAR data fusion by an enhanced version of the backward geocoding procedure.

millimetrewave domain has been discussed. Motivated by the goal to create digital surface models of densely built-up inner city areas, the full processing chain that is necessary has been shown: Starting from an exemplary sensor and navigation hardware description, via the focusing of the raw radar signals to single look complex SAR imagery up to sophisticated interferometric applications exploiting multi-baseline as well as multi-aspect configurations, a lot of interdisciplinary expertise is needed to generate competitive results. The potential of airborne single-pass multi-baseline data for time-critical mapping scenarios has been explained and state-of-the-art processing outputs have been shown. To sum up, it can be observed that both airborne and spaceborne SAR remote sensing have their distinct advantages, which can be exploited favourably subject to the specific task. Beyond that, cutting-edge airborne sensors may always be used as testing prototypes for future spaceborne missions.

Future work in the field of airborne SAR will mainly have to focus on effective utilization of only sparsely available data. Since it is expensive and cumbersome to either collect large data stacks or to equip carrier platforms with many receiving antennas, methodological developments should aim at achieving maximum information from minimum available measurements. This way the time and cost efficiency of synthetic aperture radar remote sensing will come to its full prestige, while ever improving sensor technology and increasingly sophisticated processing strategies will enable a precise and comprehensive mapping of urban areas.

References

Bamler, R. & Hartl, P., 1998: Synthetic aperture radar interferometry. – Inverse Problems **14** (4): R1–R54.

Bamler, R., Eineder, M., Adam, N., Zhu, X. & Gernhardt, S., 2009: Interferometric potential of high resolution spaceborne SAR. – PFG – Photogrammetrie, Fernerkundung, Geoinformation **2009** (5): 407–419.

Bolter, R., 2001: Buildings from SAR: Detection and reconstruction of buildings from multiple view high resolution interferometric SAR data. – PhD Thesis, Technische Universität Graz, Österreich.

Brenner, A.R., 2010: Proof of concept for airborne SAR imaging with 5 cm resolution in X-band. – 8th European Conference on Synthetic Aperture Radar: 615–618.

Danklmayer, A. & Chandra, M., 2009: Precipitation effects for Ka-band SAR. – Advanced RF Sensors for Earth Observation.

Edrich, M. & Weiss, G., 2008: Second-generation Ka-band UAV SAR system. – 38th European Microwave Conference: 1636–1639.

Essen, H., Brehm, T., Boehmsdorff, S. & Stilla, U., 2007: Multibaseline interferometric SAR at millimeterwaves – Test of an algorithm on real data and a synthetic scene. – International Archives of the Photogrammetry, Remote Sensing and Spatial Information Sciences **36** (3/W49B): 35–39.

Essen, H., 2010: Airborne remote sensing at millimeter wave frequencies. – Sörgel, U. (ed.): Radar remote sensing of urban areas. – Springer Science + Business Media.

Ferretti, A., Prati, C. & Rocca, F., 2001: Permanent scatterers in SAR interferometry. – IEEE Transactions on Geoscience and Remote Sensing **39** (1): 8–20.

Gens, R. & Van Genderen, J.L., 1996: Review article SAR interferometry – issues, techniques, applications. – International Journal of Remote Sensing **17** (10): 1803–1835.

Gernhardt, S., Adam, N., Eineder, M. & Bamler, R., 2010: Potential of very high resolution SAR for persistent scatterer interferometry in urban areas. – Annals of GIS **16** (2): 103–111.

Gernhardt, S., Cong, X., Eineder, M., Hinz, S. & Bamler, R., 2012: Geometrical fusion of multitrack PS point clouds. – IEEE Geoscience and Remote Sensing Letters **9** (1): 38–42.

Graham, L.C., 1974: Synthetic interferometer radar for topographic mapping. – IEEE **62** (6): 763–768.

Liebe, H.J., 1985: An updated model for millimeter wave propagation in moist air. – Radio Science **20** (5): 1069–1089.

Lillesand, T.M., Kiefer, R.W. & Chipman, J.W., 2004: Remote sensing and image interpretation. – 5th Edition, John Wiley & Sons.

Lord, R., 2000: Aspects of stepped-frequency processing for low-frequency SAR systems. – PhD Thesis, University of Cape Town, South Africa.

Magnard, C., Brehm, T., Essen, H. & Meier, E., 2012: High resolution MEMPHIS SAR data processing and applications. – PIERS: 328–332.

Nouvel, J.F. & Plessis, O.R., 2008: The ONERA compact SAR in Ka-band. – 7th European Conference on Synthetic Aperture Radar: 183–186, on CD.

Palm, S., Oriot, H.M. & Cantalloube, H.M., 2012: Radargrammetric DEM extraction over urban area using circular SAR imagery. – IEEE Transactions on Geoscience and Remote Sensing **50** (11): 4720–4725.

Reale, D., Fornaro, G., Pauciullo, A., Zhu, X. & Bamler, R., 2011: Tomographic imaging and monitoring of buildings with very high resolution SAR data. – IEEE Geoscience and Remote Sensing Letters **8** (4): 661–665.

Reigber, A. & Moreira, A., 2000: First demonstration of airborne SAR tomography using multibaseline L-band data. – IEEE Transactions on Geoscience and Remote Sensing **38** (5): 2142–2152.

Reigber, A., Alivizatos, E., Potsis, A. & Moreira, A., 2006: Extended wavenumber-domain synthetic aperture radar focusing with integrated motion compensation. – IEEE Proceedings Radar, Sonar and Navigation **153** (3): 301–310.

Rosen, P.A., Hensley, S., Joughin, I.R., Li, F.K., Madsen, S.N., Rodriguez, E. & Goldstein, R.M., 2000: Synthetic aperture radar interferometry. – Proceedings of the IEEE **88** (3): 333–382.

Rossi, C., Fritz, T., Eineder, M., Erten, E., Zhu, X. & Gernhardt, S., 2012: Towards an urban DEM generation with satellite SAR interferometry. – International Archives of the Photogrammetry, Remote Sensing and Spatial Information Sciences **39** (B7): 73–78.

Sauer, S., Ferro-Famil, L. & Reigber, A., 2011: Three-dimensional imaging and scattering mechanism estimation over urban scenes using dual-baseline polarimetric InSAR observations at L-band. – IEEE Transactions on Geoscience and Remote Sensing **49** (11): 4616–4629.

Schaefer, C., Völker, M., Lopez-Dekker, P., Younis, M., Dagazo-Eusebio, E. & Ludwig, M., 2012: Space-borne Ka-band across-track SAR interferometer. – 1st International Workshop on Ka-band Earth Observation Radar Missions.

Schimpf, H., Essen, H., Boehmsdorff, H. & Brehm, T., 2002: MEMPHIS – a fully polarimetric experimental radar. – IEEE International Geoscience and Remote Sensing Symposium: 1714–1716.

Schmidt, R.O., 1986: Multiple emitter location and signal parameter estimation. – IEEE Transactions on Antennas and Propagation **34** (3): 276–280.

Schmitt, M., Magnard, C., Brehm, T. & Stilla, U., 2011: Towards airborne single pass decimeter resolution SAR interferometry over urban areas. – Stilla, U., Rottensteiner, F., Mayer, H., Jutzi, B. & Butenuth, M. (eds.): Photogrammetric Image Analysis. Lecture Notes in Computer Science **6952:** 197–208.

Schmitt, M. & Stilla, U., 2011: Fusion of airborne multi-aspect InSAR data by simultaneous backward geocoding. – Joint Urban Remote Sensing Event: 53–56.

Schmitt, M. & Stilla, U., 2013a: Compressive-sensing based layover separation in airborne single-pass multi-baseline InSAR data. – IEEE Geoscience and Remote Sensing Letters **10** (2): 313–317.

Schmitt, M. & Stilla, U., 2013b: Adaptive multi-looking of airborne single-pass multi-baseline InSAR stacks. – IEEE Transactions on Geoscience and Remote Sensing: in press.

Skolnik, M.I., 1980: Introduction to radar systems. – McGraw-Hill, New York, USA.

Sörgel, U., 2010: Radar remote sensing of urban areas. – Springer Science + Business Media.

Stanko, S., Johannes, W., Sommer, R., Wahlen, A., Schröder, M. & Caris, M., 2012: SUMATRA – A UAV based miniaturized SAR system. – 9th European Conference on Synthetic Aperture Radar: 30–33.

Stilla, U., Sörgel, U. & Thönnessen, U., 2003: Potential and limits of InSAR data for building reconstruction in built-up areas. – ISPRS Journal of Photogrammetry and Remote Sensing **58** (1–2): 113–123.

Stilla, U., 2007: High resolution radar imaging of urban areas. – Fritsch, D. (ed.): Photogrammetric Week '07: 149–158.

Thiele, A., Cadario, E., Schulz, K., Thönnessen, U. & Sörgel, U., 2007: InSAR phase profiles at building locations. – International Archives of the Photogrammetry, Remote Sensing and Spatial Information Sciences **36** (3/W49A): 203–208.

Waypoint Products Group, 2013: Inertial Explorer® User Guide. Online: http://www.novatel.com/assets/Documents/Waypoint/Downloads/InertialExplorer850_Manual.pdf (17.6.2013).

Wilkinson, A.J., Lord, R.T. & Inggs, M.R., 1998: Stepped-frequency processing by reconstruction of target reflectivity spectrum. – 1998 South African Symposium on Communications and Signal Processing: 101–104.

Zhu, X. & Bamler, R., 2010: Tomographic SAR inversion by L1 norm regularization – The compressive sensing approach. – IEEE Transactions on Geoscience and Remote Sensing **48** (10): 3839–3846.

Addresses of the Authors:

Dipl.-Ing. Michael Schmitt, Univ.-Prof. Dr.-Ing. Uwe Stilla, Technische Universität München, Photogrammetry and Remote Sensing, D-80333 München, Tel.: +49-89-289-22672, -22671, Fax: +49-89-289-23202, e-mail: {michael.schmitt}{stilla}@bv.tum.de

Christophe Magnard, MSc, University of Zurich, Remote Sensing Laboratories, CH-8057 Zürich, Tel.: +41-44-6355197, Fax: +41-44-6356846, e-mail: christophe.magnard@geo.uzh.ch

Dr. Stephan Stanko, Fraunhofer Institute for High Frequency Physics and Radar Techniques FHR, D-53343 Wachtberg, Tel.: +49-228-9435-704, Fax: +49-228-9435-608, e-mail: stephan.stanko@fhr.fraunhofer.de

Dipl.-Ing. (FH) Christian Ackermann, Technische Universität München, Institute for Astronomical and Physical Geodesy, D-80333 München, Tel.: +49-89-289-23187, Fax: +49-89-289-23178, e-mail: ackermann@bv.tum.de

Manuskript eingereicht: Februar 2013
Angenommen: Juni 2013